ADVANCED FUNCTIONAL MATERIALS
www.afm-journal.de

Ambient-Dried Cellulose Nanofibril Aerogel Membranes with High Tensile Strength and Their Use for Aerosol Collection and Templates for Transparent, Flexible Devices

Matti S. Toivonen, Antti Kaskela, Orlando J. Rojas, Esko I. Kauppinen, and Olli Ikkala**

The application potential of cellulose nanofibril (CNF) aerogels has been hindered by the slow and costly freeze- or supercritical drying methods. Here, CNF aerogel membranes with attractive mechanical, optical, and gas transport properties are prepared in ambient conditions with a facile and scalable process. Aqueous CNF dispersions are vacuum-filtered and solvent exchanged to 2-propanol and further to octane, followed by ambient drying. The resulting CNF aerogel membranes are characterized by high transparency (>90% transmittance), stiffness (6 GPa Young's modulus, 10 GPa $cm^3\ g^{-1}$ specific modulus), strength (97 MPa tensile strength, 161 MPa $m^3\ kg^{-1}$ specific strength), mesoporosity (pore diameter 10–30 nm, 208 $m^2\ g^{-1}$ specific surface area), and low density (≈0.6 g cm^{-3}). They are gas permeable thus enabling collection of nanoparticles (for example, single-walled carbon nanotubes, SWNT) from aerosols under pressure gradients. The membranes with deposited SWNT can be further compacted to transparent, conductive, and flexible conducting films (90% specular transmittance at 550 nm and 300 Ω $\square^{-1}$ sheet resistance with $AuCl_3$-salt doping). Overall, the developed aerogel membranes pave way toward use in gas filtration and transparent, flexible devices.

1. Introduction

Aerogels are porous, low density (0.8–0.001 g cm^{-3}) solid materials with a high specific surface area; they have been recognized as promising materials for a plethora of applications, such as transparent thermal or acoustic insulation, membrane separation, lightweight construction, supported catalysis, superabsorbency, and water purification.[1–10] Advanced materials such as optical elements for refractive index matching, low dielectric coefficient substrates for electronics, encapsulation media, sensors, actuators, conductors, mechanical energy absorbers, and energy storage have been developed from aerogels.[1–3,5,9–19] A desirable combination of properties for many of the applications cited include transparency, high porosity (>50 vol% air), and mechanical strength.

Aerogels prepared from inorganic compounds, most often silica, display transparency and porosity, but classically suffer from brittleness.[3,20] This is a result of weak interlinks between the nanoparticles that compose the aerogel skeleton.[21] One promising approach is reinforcing the "necklace" of inorganic nanoparticles with organic components.[21–24] A possibly more facile option for constructing aerogels of high mechanical performance is using colloidal 1D or 2D building blocks, such as nanocelluloses,[13,25–28] clay,[29–32] carbon nanotubes,[5,15,33–35] or graphene.[35,36] These nanomaterials do not contain such weak interlinks within the "necklaces", thus enabling preparation of mechanically strong aerogels with no need for chemical modification.[13] The feasible mechanical properties are typically observed under compression, but generally aerogels are associated with low mechanical strength in tension. Also, transparency has remained elusive for most of the work related to nanofibrillar aerogels. Transparency is necessary for many applications but it is only possible with materials that do not absorb visible light, such as cellulose, nor scatter significantly, which is achieved by limiting aggregation to nanoscale structures.

A crucial step in the preparation of aerogels is the removal of the liquid phase, for example, via supercritical drying or freeze-drying, without disrupting the original network structure.[3,20] These drying processes can limit the production scalability as they inherently involve slow batch processing, demand specialized equipment, and operation at extreme pressures and temperatures.[20] More recently, ambient drying of aerogels has become relevant in silica aerogels after the technique was introduced in 1995 by Prakash et al.[37–39] This route relies on reinforcement of the silica gel skeleton prior to drying by suitable chemistry, suppression of cross-linking reactions, and reduction of the capillary pressure during drying by surface modification and solvent exchange.[39] In order to make feasible a more broad utilization of aerogels their scalable production needs to be resolved and ambient drying is an attractive solution.

M. S. Toivonen, Prof. O. Ikkala
Molecular Materials
Department of Applied Physics
Aalto University School of Science
P.O. Box 15100, FIN-00076 Aalto, Espoo, Finland
E-mail: olli.ikkala@aalto.fi

Dr. A. Kaskela, Prof. E. I. Kauppinen
Nanomaterials Group
Department of Applied Physics
Aalto University School of Science
P.O. Box 15100, FIN-00076, Aalto Espoo, Finland
E-mail: esko.kauppinen@aalto.fi

Prof. O. J. Rojas
Bio-Based Colloids and Materials
Department of Forest Products Technology
Aalto University School of Chemical Technology
P. O. Box 16300, FIN-00076 Aalto, Finland

DOI: 10.1002/adfm.201502566

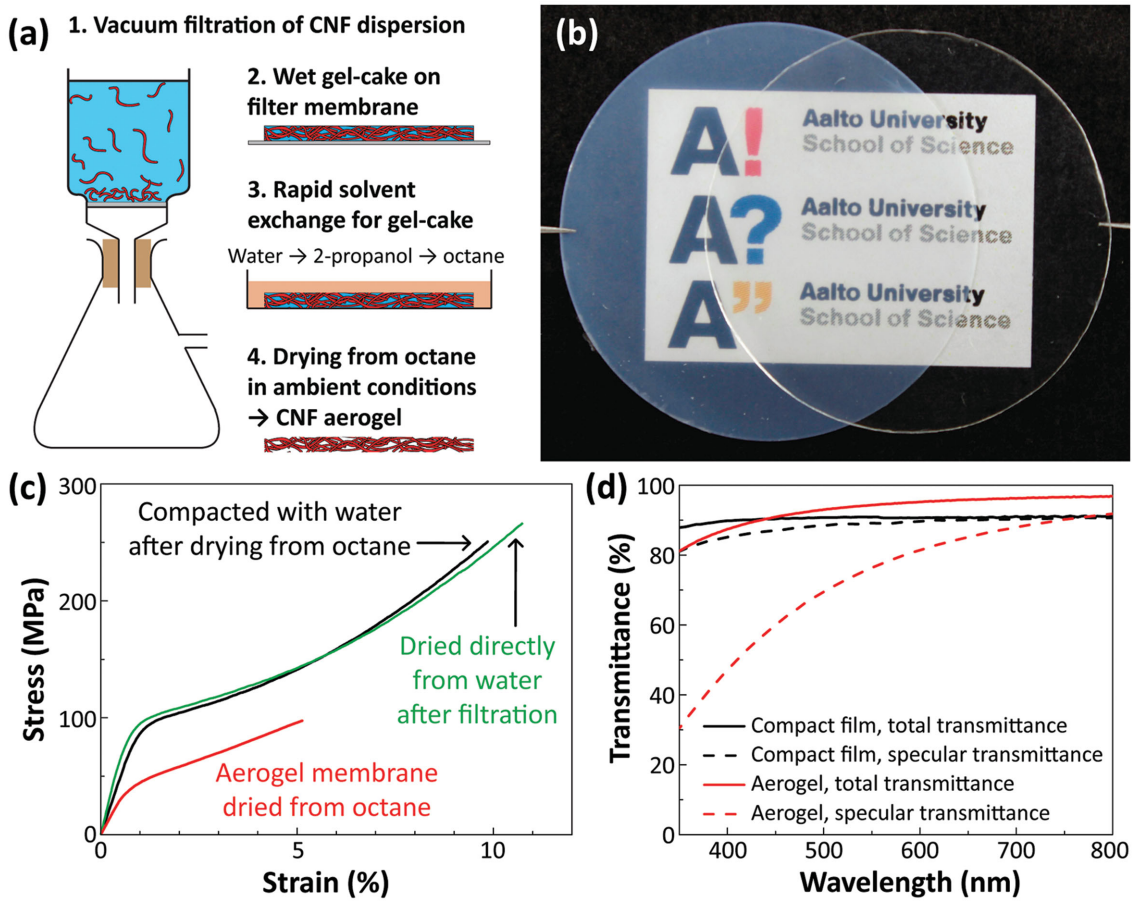

Figure 1. Preparation and properties of CNF aerogel membranes and compacted CNF films. a) Schematic illustration of the preparation of CNF aerogel membranes. b) Photograph of CNF aerogel membrane (left, ≈25 µm thick) and compacted film (right, ≈12 µm thick). c) Tensile stress–strain curves of aerogel membrane, CNF film compacted with water from the aerogel and CNF film dried directly from water after filtration. Tensile characterization is carried out at 50% relative air humidity. d) UV–vis spectra of total and specular transmission through CNF aerogel membrane and compacted film.

Cellulose nanofibrils (CNF also denoted as cellulose nanofibers, nanofibrillated cellulose, NFC) have drawn significant attention in recent years due to the fact that they exhibit a desirable combination of properties such as high mechanical properties (i.e., elastic modulus of 29–36 GPa and tensile strength 1–3 GPa in the longitudinal direction for individual fibrils), high transparency in films, renewability, availability, and potential biocompatibility.[40–44] Previously CNF have been used to prepare tough and flexible aerogels by freeze-drying and supercritical drying.[13,25–28] Transparent CNF aerogels have been recently shown to be possible by using TEMPO-oxidized CNF and supercritical CO_2 drying.[26,28] Porosity of films of microfibrillated cellulose can be increased if dried from organic solvents, for example, a 21% increase in porosity has been achieved upon drying from acetone at 55 °C under compression.[45] Surprisingly, to date, no ambient drying of CNF aerogels has been reported.

Aerogel membranes, in contrast to bulk aerogels, could offer the possibility to allow substantial gas flow through and enable filtration or collection of aerosol particles. A valuable line of application for this property, as demonstrated in this work, is the preparation of flexible, transparent, and conductive aerogel membranes, and further compacted films, by collecting directly on the aerogel substrate high-quality single-walled carbon nanotubes (SWNTs) obtained from aerosol synthesis. SWNT networks are promising components for a variety of flexible electronics applications.[46,47] SWNT networks show potential to replace the current industry standard material indium-tin oxide (ITO) in applications of high value such as touch sensors with improved flexibility, while enabling maximum transparency and high raw material availability.[48–50] In continuation, more complex devices can be fabricated by patterning and further processing of the conductive SWNT network.[51–53] As a fascinating direction of further research, biocompatibility of CNF may open possibilities in completely new biomedical devices for cell culturing, neurotransmitter monitoring, and conformable, responsive biosensors.[54–57]

Here, we report on the preparation of gas-permeable, transparent, and mesoporous CNF aerogel membranes that display high strength, remarkably in tension, and high stiffness, through ambient drying after solvent exchange, i.e., not needing freeze-drying or supercritical drying. We further demonstrate their use as a platform for transparent, flexible conductive films upon collection of SWNTs from an aerosol synthesis stream. We characterize the relevant properties of the aerogel membranes for filtration and, if needed, show their ability to turn into dense and transparent films upon rewetting and drying from water. The tensile and optical properties of the

aerogel membranes and those of the compacted film with and without SWNTs are characterized. In addition, we determine the electrical properties of the CNF/SWNT hybrid films under mechanical deformation.

2. Results and Discussion

Gas-permeable, mesoporous, and transparent CNF aerogel membranes were prepared by vacuum filtration of an aqueous CNF dispersion followed by solvent exchange of the formed gel-cake from water to 2-propanol and further to octane, followed by drying in ambient conditions, as summarized in **Figure 1**a. The solvent exchange process took ≈20 min for completion. Slow drying of the resulting stiff CNF-in-octane organogel on a smooth support resulted in a transparent CNF aerogel membrane, as shown on the left in the photograph in Figure 1b. By contrast, if the CNF aerogel membrane was re-wetted with water and allowed to dry from water, a transparent, compacted CNF film resulted, as shown on the right in Figure 1b. Upon such spontaneous, capillary compaction the thickness of the membranes typically halved. No lateral shrinkage of the membranes was observed upon drying from either octane or water. The in-plane alignment of the CNF network along the lateral dimensions of the filtered gel-cake is likely to contribute to the resistance to shrinkage as this anisotropy makes the in-plane direction stronger compared to the case of an isotropic, unfiltered gel. This is supported by easily observable shrinkage of a nonfiltered CNF gel (2.1 wt%) upon drying from octane after a comparable solvent-exchange process (see Figure S1, Supporting Information), although a difference in concentration might be another relevant factor.

The density of the CNF aerogel membrane was ≈0.6 g cm^{-3} and the density of the compacted film was 1.5 g cm^{-3} as defined by mercury porosimetry. The BET specific surface area of the CNF aerogel membranes was ≈208 m^2 g^{-1} and the majority of pores were of the order of 10–30 nm in diameter as determined by nitrogen physisorption. The adsorption isotherms and BJH pore size distributions are shown in Figure S2 (Supporting Information). The specific surface area is remarkably high as it is of the same order and in some cases higher than that of the CNF aerogels prepared by freeze- or supercritical CO_2 drying.[13,25–27] These results clearly show that even without any surface modification or cross-linking CNF aerogels can be prepared by a facile and rapid solvent exchange process followed by ambient drying. If needed, it is likely that lower density and higher pore size are possible by strengthening and stiffening the CNF gel prior to drying, for example, by chemical or supramolecular cross-linking.[39,58]

The small size of the pores and the absence of large aggregates is evident also in the representative SEM images of top surfaces and fracture surfaces of both CNF aerogel membranes and compacted films (see **Figure 2**), where no large voids or aggregates are observed. The pore size is too small to be seen

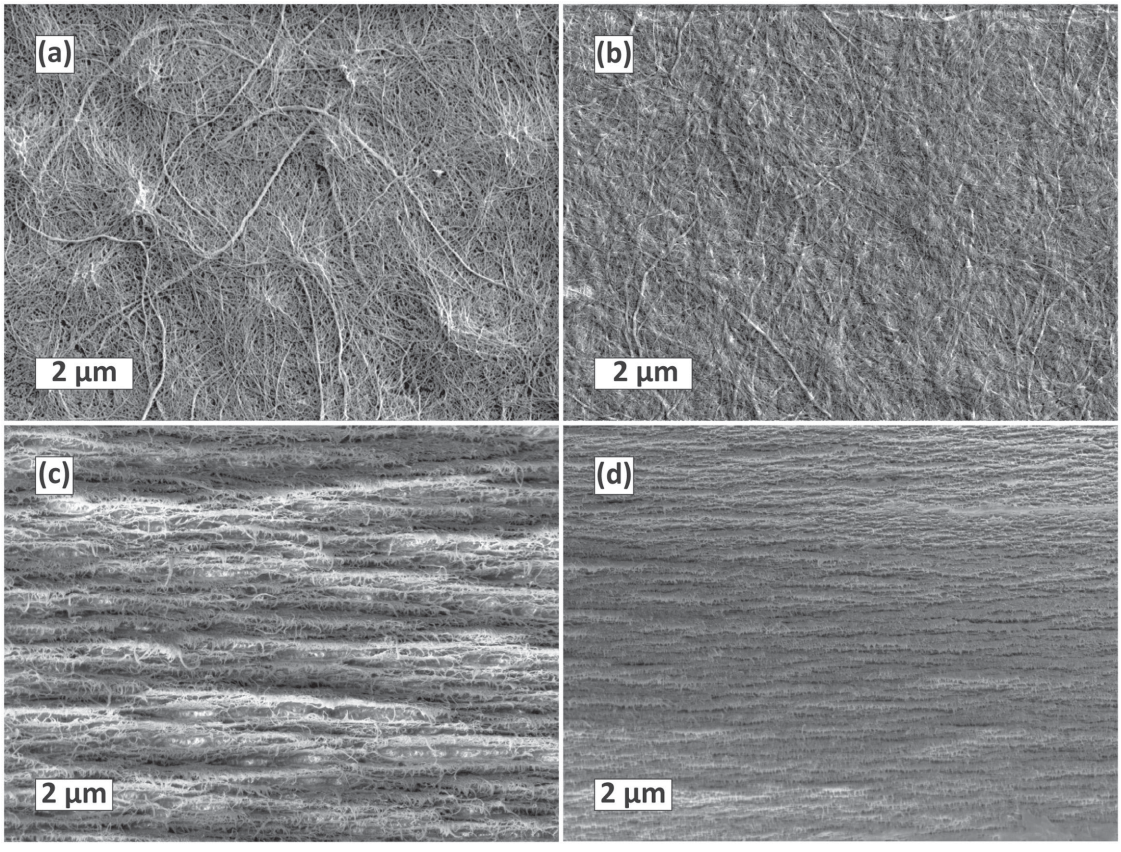

Figure 2. SEM plane view images (above) of a) a CNF aerogel membrane, and b) a compacted CNF film. Fracture surfaces (below) resulting from tensile rupture of c) an aerogel membrane, and d) a compacted CNF film are also shown as SEM cross-sections.

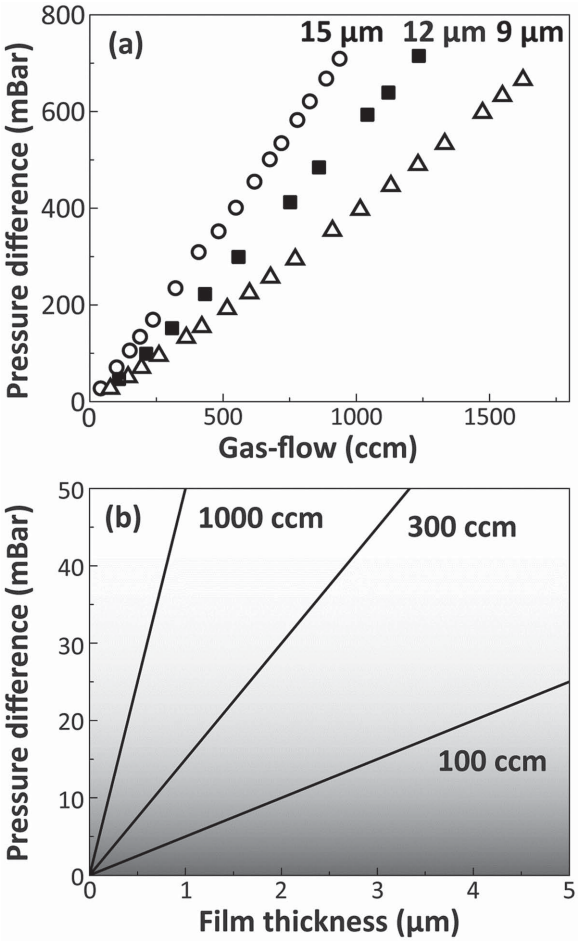

Figure 3. Gas permeability of CNF aerogel membranes. a) Pressure difference over the CNF aerogel membranes (diameter 45 mm) as a function of gas flow (cubic centimeters per minute, ccm). Thicknesses of membranes were 9 (open triangles), 12 (filled squares), and 15 (open circles) µm. The measurements were carried out at 20 °C and with pressurized, dry air. b) Extrapolated design curves for selection of appropriate thickness of the CNF aerogel membrane for an appropriate combination of pressure difference over the membrane with three different values of gas flow. Darker shaded region is the area of pressure differences which can be considered relevant for large-scale gas filtration applications.

clearly from SEM images. The fracture surface of the aerogel had a lamellar morphology as is typically observed in CNF films but, somewhat surprisingly, the average thickness of CNF lamellae is clearly larger in the fracture surface of the CNF aerogel membrane in comparison to that of the compacted CNF film. The reason for this is not clear, but it might be suggested that increased porosity correlates with increased lamellar thickness at the fracture surface.

The tensile behavior of the compacted CNF films dried directly from water, the aerogel membrane and the compacted film are shown in Figure 1c and the mechanical properties are summarized in Table S1 (Supporting Information). The tensile stress–strain curve of the film after compacting is practically indistinguishable from that of the films dried directly from water, suggesting that the CNF fibrils are not altered by the solvent exchange process or drying from octane and the structure of the transparent film resulting from compacting with water is very similar to a transparent film dried directly from water without any solvent exchange. Not surprisingly, taken the external dimensions of the sample, the aerogel membrane shows reduced nominal Young's modulus, ultimate tensile strength, and maximum strain when compared to the compact films, which is explained by the lower density of the former. Nonetheless it is important to note that the strength of roughly 100 MPa and Young's modulus of 6 GPa are very high for an aerogel, which cannot typically even be tested in tension. Dividing the stresses by corresponding material densities gives more proper account of the porosity effect, and the resulting specific strength of the aerogel membrane is 36% larger than that of the compacted film, see Figure S3 and Table S1 (Supporting Information). A possible explanation for this could be a higher density of the junction points of the fibrils compared to the mass density in the aerogel than the compact film.

The gas permeability of the CNF membranes was evaluated by measuring the gas flow rate under applied pressure difference over the CNF aerogel membranes (circular with a diameter of 45 mm) with thicknesses of 9, 12, and 15 µm. The gas flow rate correlates linearly with the pressure drop over the aerogel membrane as shown in **Figure 3**a. As could be predicted by Darcy's law (see Equation S1, Supporting Information), the slopes of such flow profiles correlate linearly with the thickness of the aerogel membrane. The mesoporous CNF aerogel membranes are likely to exhibit a high particulate retention efficiency which may make them attractive for gas filtration applications. However, the pressure difference necessary for a given gas flow may be over tenfold higher than that of traditional gas filtration membranes, which reduces the suitability of the present relatively thick free-standing aerogel membranes tested here for large-scale gas filtration. But the linear relationship between the pressure difference and membrane thickness allows the extrapolation of the proper thickness of the aerogel membranes according to applications aimed. If thin aerogel membranes are required, an option is to use a macroscopic support membrane on top of which the CNF aerogel membrane is deposited. Extrapolated design curves for selection of appropriate CNF aerogel membrane thickness at constant gas flow values are shown in Figure 3b. A proof of concept for these self-standing membranes can here be ascertained to collect SWNTs from an aerosol synthesis process, as discussed in the next section.

SWNTs (see Figure S4, Supporting Information) were synthesized in the gas-phase floating catalyst-chemical vapor deposition (FC-CVD) process and collected from the process stream directly on the CNF aerogel which was subsequently washed with acetonitrile and compacted by drying from a 1:1 (w/w) water–acetonitrile mixture. The resulting CNF/SWNT hybrid films are highly conductive and transparent (see **Figure 4** and Figure S5, Supporting Information). The FC-CVD synthesis and collection of the ready SWNT network enables straightforward fabrication of high performance, flexible transparent, and conductive films (TCF) while avoiding the complex, costly, and often detrimental liquid dispersion steps relying on high-intensity sonication in surfactant solutions, which reduce integrity and performance of SWNT TCFs.[50,59] In previous works

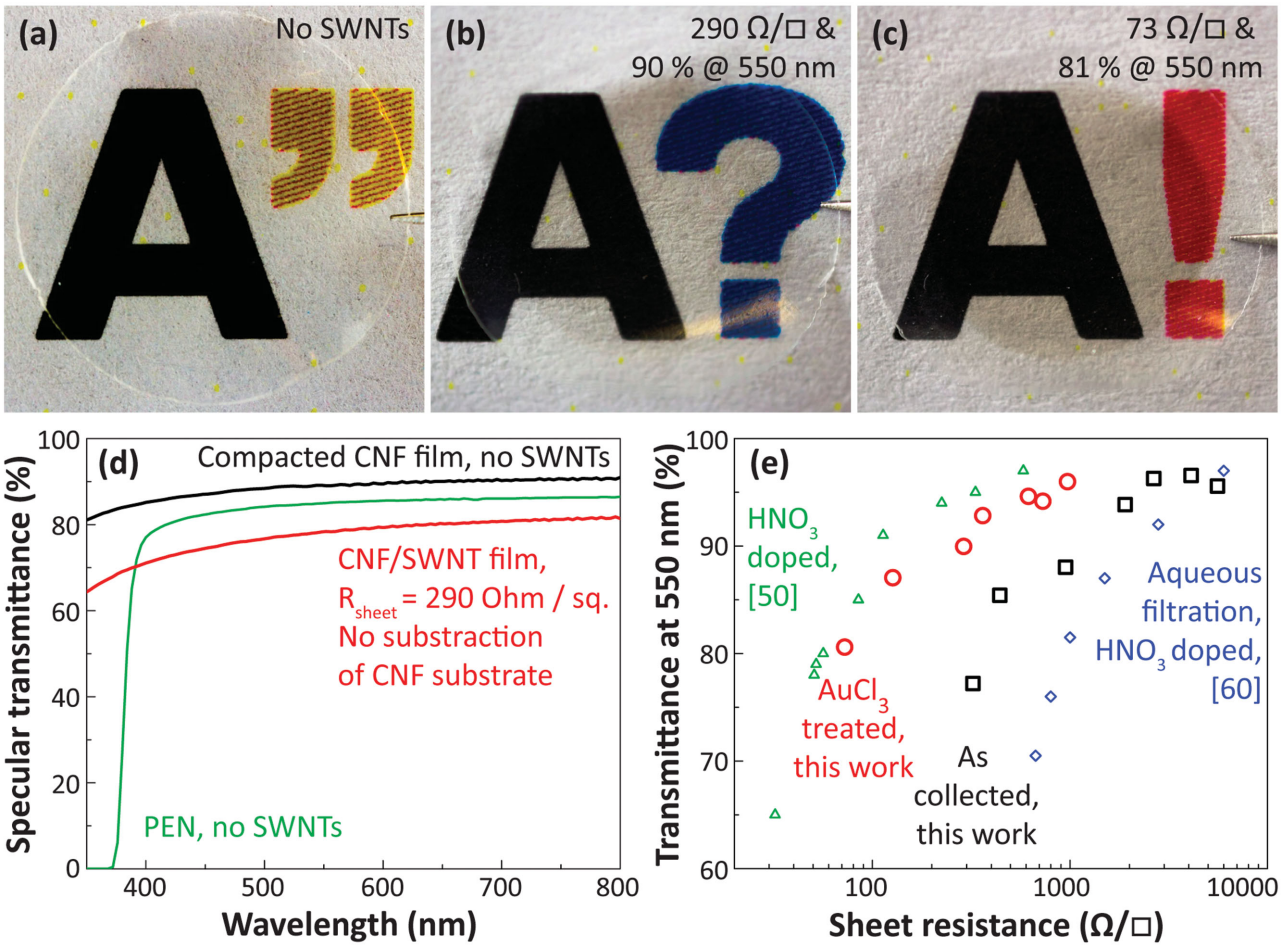

Figure 4. Photographs of a) reference CNF (diameter 12 mm) and b,c) CNF/SWNT films with low sheet resistances in $\Omega\ \square^{-1}$ (Ohm per square) of SWNT networks after compacting, d) UV–vis spectra of CNF reference film, a representative CNF/SWNT film and a PEN film for comparison, and e) specular transmittances at 550 nm versus sheet resistances of SWNT networks without doping (black squares) and after gold-salt doping (red circles). For comparison data from relevant works of Kaskela et al. (green triangles) and Koga et al. (blue diamonds) are shown.[50,60] Transmittance at 550 nm in e) is measured by using a pure substrate as a reference.

the SWNT network has been collected on a filter and transfer of the delicate network to the final substrate has been necessary.[50] Using a compactable aerogel membrane eliminates the latter step, thus improving processing efficiency and reducing material consumption and the risk of breaking the SWNT network.

The CNF/SWNT hybrid film's sheet resistance was further reduced by a factor of 0.23 by gold salt doping, resulting in a coefficient of light transmittance at 550 nm versus sheet resistance that are in the same order of magnitude as the highest reported values in the literature for SWNT networks (see Figure 4e, where relevant comparisons are drawn). The combination of high conductivity and transparency is a result of high connectivity of the SWNT network with minimal thickness. The structure of the CNF/SWNT hybrid film is shown in the SEM images in **Figure 5**.

The sheet resistance of narrow strips of CNF/SWNT hybrid films was monitored in situ using the two-point resistance method during stretching in uniaxial tension with maximum strain increasing in a step-wise manner (**Figure 6**a), cyclic stretching in the elastic area (Figure 6c), and bending (Figure 6b,d). Figure 6a shows clearly that the resistance increases slightly with strain and if the deformation is not reversible, neither is the change in resistance. When the tensile strain was cycled in the elastic regime from 0% to 0.5%, the resistance correlated (0.5% increase in resistance) with strain and seemed fully reversible on the scale of tens of cycles. After several thousand cycles a small irreversible change (3.5% after 2900 cycles) in resistance was observed.

During bending the distance between the clamped ends of the sample (i.e., gauge length) was cycled from the original length of 10 to 2.5 mm and back. The radius of curvature in the middle of the film (indicated by white circles in insets of Figure 6d) cyclically reduced down to 0.6 mm. There was a small increase of resistance (<1% per cycle) with bending which was largely, but not completely reversible. The sheet resistance drifts to slightly higher values with repeated cycling. The behavior of the SWNT network conductivity on a CNF substrate during mechanical deformation has not been reported previously, but a similar drift behavior has been observed on a different substrate material. In stretchable polydimethylsiloxane/carbon nanotube (CNT) conductors under tensile cycling a

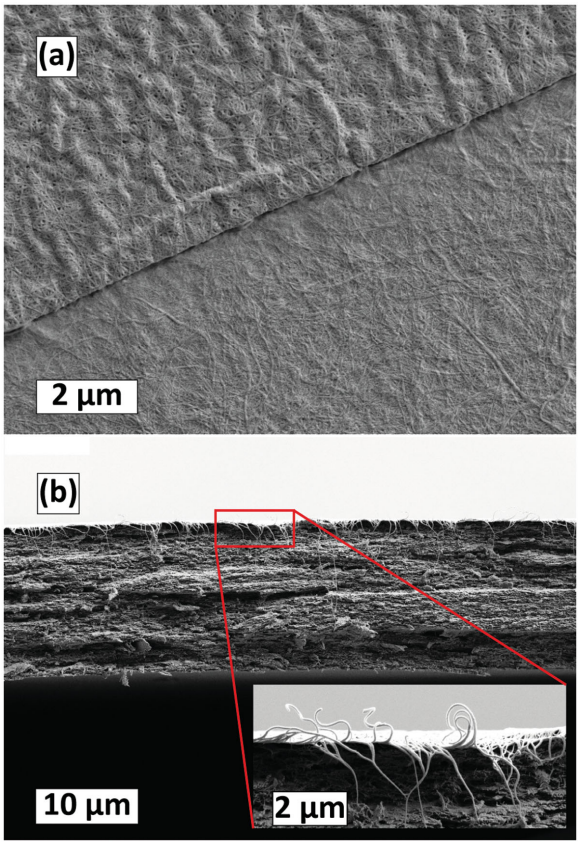

Figure 5. SEM images of compacted CNF/SWNT hybrid film a) plane view at the edge of the SWNT-network where SWNT network is shown on upper left and CNF network on the lower right, and b) at the fracture surface with inset showing thin SWNT network on top of the CNF film.

similar drift has been observed and shown to level off to a given value if maximum strain is not increased.[61] The mechanism suggested to explain this behavior is the reduction of interconnects between CNTs due to stress localization leading to debonding between CNTs. The same explanation seems applicable to the present system.

3. Conclusion

CNF aerogel membranes were prepared through a facile and scalable fabrication process consisting of filtration, solvent exchange, and drying in ambient conditions, notably avoiding the costly freeze- or supercritical drying processes. The CNF aerogel membranes were transparent, gas-permeable, mesoporous, and exhibit high mechanical properties in tension, which is otherwise rarely achieved. The potential of the CNF aerogel membranes for application in preparation of transparent, conductive films is demonstrated by deposition of SWNTs via aerosol filtration from synthesis processes. The CNF/SWNT hybrid films after compacting with water show high transparency and good mechanical properties combined with low sheet resistance. This allows design options toward flexible devices, combining the electrical and sensing properties of carbon nanotubes, the filtration and trapping properties of aerogels, and biocompatibility and sustainability of nanocelluloses.

4. Experimental Section

Materials: CNF was prepared from never dried birch pulp by disintegrating the pulp 12 times through a fluidizer (Microfluidics Corp., Newton, MA, USA) leaving a hydrogel with a consistency of ≈1.54 wt%. The CNF gel was diluted to 0.3 wt% by adding deionized water followed by vigorous stirring for 24 h. The diluted CNF dispersion was then centrifuged at 5000*g* for 60 min to remove aggregates. The sediment was discarded and the supernatant was used for sample preparation. The resulting dispersion has fibrils of diameter 5–20 nm and above due to higher aggregates and some imperfectly fibrillated material (see Figure S6, Supporting Information). The mass concentration of CNF in the obtained supernatant was determined by weighing a given amount of the dispersion and drying it overnight in an oven at 50 °C under ambient pressure followed by weighing. The final dry mass was divided by the initial mass of the dispersion to yield the reported mass percentage of the CNF dispersion. The values obtained were in the range of 0.10–0.15 wt%. The used supernatant is referred to as CNF in the text.

100 µm thick Teijin-DuPont 65FA (Teijin DuPont, Japan) was used as reference for comparison of transparent CNF films with industrially produced high transparency optoelectronics substrate material.

Ethanol (Etax Aa > 99.7 vol%) was purchased from Altia. $AuCl_3$ used for chemical doping of the SWNT electrodes, acetonitrile, 2-propanol, and octane were purchased from Sigma-Aldrich. Gas precursors for SWNT synthesis, namely carbon monoxide (CO, 99.5% purity), hydrogen (H_2, 99.999% purity), and ethylene (C_2H_4, 99.99% purity) were purchased from Aga Oy. Ferrocene (99% purity) was used as catalyst precursor, mixed in 1:4 weight ratio with silica sand, purchased from Stream Chemicals and Sigma-Aldrich, respectively.

Preparation of Mesoporous, Gas-Permeable CNF Aerogel Membranes: Typically, 80 mL of 0.1 wt% CNF dispersion was vacuum filtered on a hydrophilic polyvinylidene fluoride filter membrane (90 mm diameter, 0.45 µm pore size, GVWP, Millipore) until a wet gel-cake was formed and no flow of free water was observed, when the apparatus was tilted slightly. The filtration step was completed typically in 15 min. The filter and gel-cake were carefully transferred to a glass Petri dish and ethanol was pipetted to the edge of the filter paper before drying of the gel-cake occurred, while avoiding excessive mechanical disturbance to the gel-cake, until both were fully immersed in ethanol. After ≈5 min soak in ethanol, the filter and gel-cake were inverted onto a smooth polytetrafluoroethylene (PTFE) sheet leaving the gel-cake resting on the PTFE and the filter membrane on top. A small amount of ethanol was pipetted on the gel-cake to avoid drying and the filter membrane was carefully peeled from the gel-cake and discarded. The gel-cake was covered with 2-propanol for typically 5 min to exchange the remaining water and ethanol in the gel-cake to 2-propanol after which the used 2-propanol was discarded and new was added. This was repeated three times. After solvent exchange to 2-propanol, the same procedure was repeated using octane. After the gel-cake was soaked three times in octane, the excess octane was discarded and the gel-cake was left to dry slowly on the PTFE sheet in ambient conditions while partially covered with a glass Petri dish. During all soaking steps, the gel-cake and solvent were covered with an inverted Petri dish to avoid drying.

Preparation of Porous Bulk Sample: 2.11 wt% CNF gel was placed in a Petri dish and solvent exchange was performed as described above for vacuum filtered gel-cakes with the difference that each immersion step was 24 h long instead of 5 min. Drying was performed in ambient conditions in the Petri dish where the gel was throughout the solvent exchange process without mechanically disturbing the gel.

Compacting Gas-Permeable CNF Aerogel Membranes with Water: Dry CNF aerogel membranes were placed on smooth PTFE sheet and a small amount of water was pipetted on it to wet the membrane. When

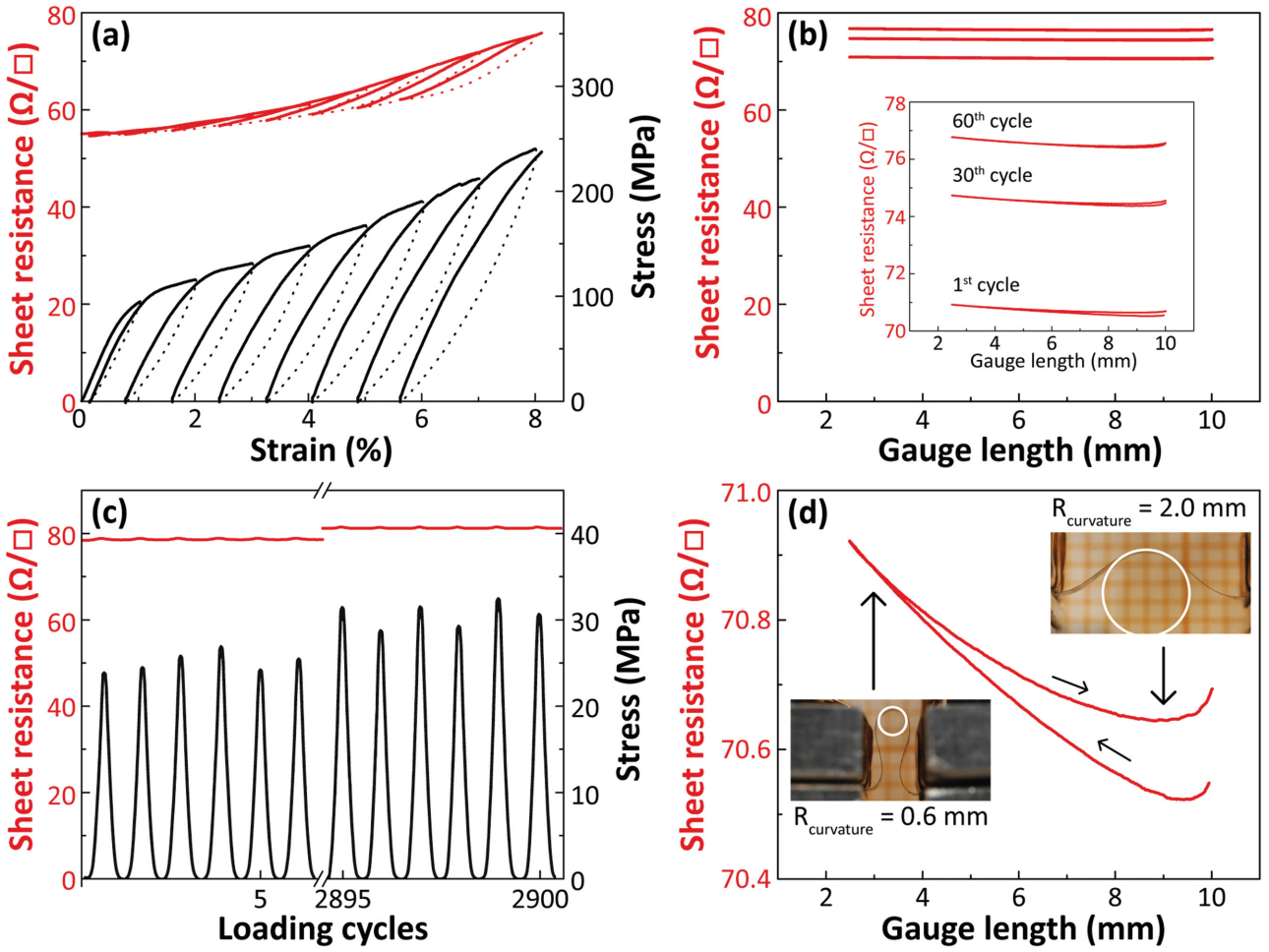

Figure 6. Development of sheet resistance and stress of conductive CNF/SWNT film with tensile strain a) with increasing cyclic strain, b) sheet resistances of CNF/SWNT film for 1st, 30th, and 60th bending cycle with inset after rescaling of the y-axis, c) repeated cyclic tensile straining in the elastic area of the CNF film, and d) during a single bending cycle (1st cycle in b) with photos of side view as insets and respective radii of curvature, which is also illustrated by the white circles in the photos.

the whole membrane was wetted, the excess water was removed, and the membrane was left to dry slowly in ambient conditions on the PTFE sheet.

Ultraviolet–Visible Light (UV–vis) Spectroscopy: Transmission spectra of CNF aerogel membranes, compacted CNF films, compacted CNF/SWNT hybrid films, and commercial PEN films were recorded in UV–visible range with PerkinElmer Lambda 950 UV/vis/NIR absorption spectrophotometer. Aerogel membranes were roughly 25 µm and compacted CNF films 12 µm thick. All spectra without SWNT network were recorded without a sample in the reference beam. Spectra of SWNT network alone was extracted by removing CNF-reference film background. Specular transmittance was recorded with a detector directly in the line of the specular beam. Total transmittance was recorded using a 150 mm integrating sphere.

Scanning Electron Microscopy (SEM): Pieces of CNF aerogel membranes, compacted CNF films, and compacted CNF/SWNT hybrid films were attached to aluminum SEM stubs with carbon tape and sputtered with ≈10 nm thick gold film (Emitech K100X). Imaging was carried out with a Zeiss Sigma VP scanning electron microscope at 1–2 kV acceleration voltage. Samples for imaging of fracture surfaces were first fractured in uniaxial tension during tensile characterization.

Characterization of Gas Permeability: Circular pieces of CNF-aerogel membranes with diameters of 47 mm and varying thicknesses were placed in a flow-through aerosol collection chamber supported by a stiff steel mesh from behind. The chamber was sealed so that a rubber ring tightened the CNF aerogel membrane against the steel mesh leaving a circular area with a diameter of 45 mm exposed for the pressurized air. The pressure difference over the aerogel membrane was measured with a manometer (HD 2164.0 from Delta Ohm). The gas flow was measured with an air flow calibrator (Gilibrator 2 from Sensidyne equipped with Standard Flow Cell). Measurements were carried out at 20 °C and the used gas was dry pressurized air.

Specific Surface Area and Pore Size Distribution by Nitrogen Adsorption: The Brunauer–Emmett–Teller specific surfaces area (BET) was determined by N_2 physisorption using a Micromeritics TriStar II automated system.[62] 70–90 mg of the gas-permeable CNF aerogel membrane was dried for 2 h under dry nitrogen gas flow at 70 °C in the measurement vessel prior to the analysis. This analysis was repeated for three identically prepared membranes. 210 mg of compacted CNF film was prepared for analysis similarly. For analysis the dry sample and measurement vessel were transferred to the measurement apparatus and further stabilized for 2 h at 0.001 kPa vacuum. BET analysis was carried out for a relative N_2 vapor pressure of 0.003–0.950 at –196 °C. Pore size distribution was determined from the adsorption isotherm according to Barrett–Joyner–Halenda (BJH) analysis.[63]

Density Determination: Densities of the aerogel membranes were measured with mercury porosimetry using Pascal 140 and Pascal 440 porosimeters for the pressure ranges 0 to 300 kPa and 100 kPa to 400 MPa, respectively.

Synthesis of SWNTs and Collection on a Porous CNF Aerogel Membrane: SWNTs were synthesized by using continuous FC-CVD process and subsequent filtration through a mesoporous CNF aerogel membrane. Synthesis process is based on catalytic decomposition of carbon precursor gases in elevated temperatures above 1000 K on the surface of small diameter (2–5 nm) iron catalyst nanoparticles. Details on the synthesis process and reactor design are described elsewhere.[50,54] Shortly, the FC-CVD process is the following: a 100 cm^3 min^{-1} flow of carbon monoxide (CO, 99.5% purity, Aga Oy) is passed through a ferrocene saturator, filled with ferrocene (99% Stream Chemicals) and coarse grained silica sand (Sigma-Aldrich) mixed in 1:4 weight ratio to maintain high porosity and enable gas flow. Ferrocene has partial vapor pressure of 0.7 Pa at room temperature (24 °C) and it sublimes to the passing gas flow. The ferrocene containing gas flow is mixed with 150 cm^3 min^{-1} of clean CO to control the concentration of catalyst precursor and 1.5 cm^3 min^{-1} of ethylene (C_2H_4, 99.99% purity, Aga Oy) and 70 cm^3 min^{-1} flow of hydrogen (H_2, 99.999% purity, Aga Oy) to enhance reactivity. The gas mixture is injected through a water-cooled stainless steel injector into quartz walled tube furnace (length 870 mm, reactor tube diameter 22 mm) operated at maximum temperature of 1370 K. An additional CO flow of 100 cm^3 min^{-1} was introduced to between injector and quartz tube to prevent recirculation in the heating zone after the injector. Ferrocene thermally decomposes in the rapidly increasing temperature gradient as the gas flow exits the injector, leading to formation of supersaturated iron vapor, which condenses and nucleates iron nanoparticles serving as catalyst for SWNT growth. Carbon precursors, CO and C_2H_4 start to catalytically decompose on the iron catalyst nanoparticles, leading to SWNT growth, while the catalyst particles and growing SWNTs are floating in the laminar gas flow. The SWNTs can be separated from carrier gas at the reactor outlet by simple membrane filtration to form a randomly oriented SWNT network on the filter surface. Presence and structure of single-walled nanotubes has been confirmed with optical spectroscopy, SEM, TEM, and electrical transport measurements.

Washing and Compacting of CNF/SWNT Hybrid Films: After collection of SWNTs on the CNF aerogel membranes from the aerosol process, the membrane was washed with acetonitrile followed by a small amount of 1:1 (w/w) acetonitrile–water mixture. After washing the CNF/SWNT hybrid membrane with acetonitrile, a small amount of 1:1 (w/w) acetonitrile–water mixture was pipetted on the membrane and left to dry by slow evaporation.

Chemical Doping of CNF/SWNT Hybrid Films: Chemical doping of CNF/SWNT hybrid films with gold-chloride solution was used in order to further reduce the electrical sheet resistance of conductive SWNT network.[64] For the doping treatment 100 mM solution of $AuCl_3$ in acetonitrile was prepared and drop-cast on the SWNT network, until the SWNT network was completely immersed in the dopant solution. After a 5 min exposure the dopant solution was washed away with acetonitrile followed by drying under gentle nitrogen gas stream.

Transmission Electron Microscopy: High-resolution transmission electron microscopy (TEM) was used for imaging and verification of presence of single-walled carbon nanotubes and for estimation of diameters of CNF used. Observation was carried out by using a field emission TEM with double-Cs aberration correctors (JEOL JEM-2200FS operated at 80 kV).

The SWNT samples were collected on holey carbon coated copper grids (Agar Scientific), which were placed on a filter membrane at the reactor outlet for rapid (5–10 s) sample deposition in order to deposit thin, electron transparent layer to enable TEM observation.

The CNF samples were prepared by pipetting 3 µL of 0.01 wt% CNF dispersion onto a copper TEM grid with a holey carbon film and allowed to stand for 60 s before draining the excess by blotting. After blotting the sample was allowed to dry for 30 min in ambient conditions.

Tensile Characterization of CNF Aerogel Membranes and Compact Films: The CNF aerogel membranes, the compacted CNF films, and the CNF film dried directly from water after filtration were cut into strips 2.25 mm wide and more than 1.5 cm long by pressing with a custom made razor blade jig, where multiple flat blades are evenly spaced by flat metal spacers and tightened parallel to each other. For clamping, the strips were glued from both ends onto small pads of abrasive paper (ca. 3 × 4 mm) leaving a 10 mm long strip available for standard tensile tests. The widths of the strips were measured with an optical microscope (Leica MZ6 equipped with a Leica DFC420 camera). The thicknesses of the films were measured with a film thickness measurement setup composed of a displacement sensor (LGF-0110L-B, Mitutoyo), digital reader (EH-10P, Mitutoyo), and a measuring table with support for sensor (215-514 comparator stand, Mitutoyo). Samples were equilibrated at 50% relative humidity and 20 °C in a custom-made humidity chamber inside which also the tensile tester (Tensile/Compression Module 5 kN with 100 N load cell, Kammrath & Weiss GmbH) was located. Rate of elongation was 0.5 mm/ min^{-1} and gauge length was 10 mm.

In Situ Monitoring of Resistance of CNF/SWNT Hybrid Films during Mechanical Deformation: Mechanical samples were prepared from the compacted CNF/SWNT hybrid films similar to those prepared of CNF films described above. All tests were carried out at 50% relative humidity and at 20 °C. The sheet resistance of the SWNT network was measured from several points with a four-point measurement apparatus (Jandel RM3000) on the film prior to cutting of the strips. The apparatus used was the same as for tensile characterization, but the clamps used were exchanged for ones where the top clamp was insulated from the sample by Kapton tape. A strip of copper tape 4 mm wide was attached on the Kapton tape to work as the electrode for connecting the SWNT network and connect it to the wiring to the resistance measurement apparatus. The contact resistance between the copper tape electrodes and the SWNT network was estimated to be negligible as the sheet resistances obtained after correcting the measured two-point resistance with the shape factor of the sample was approximately the same as that obtained by four-point measurement of the film prior to cutting of samples. Two-point resistance was measured using a digital multimeter (Agilent 34410A 6½ Digit Multimeter).

For bending the samples the distance between the clamped ends was cycled between the starting gauge length of 10 and 2.5 mm at a rate of 20 µm s^{-1} during which the load-displacement curves were recorded simultaneously with two-point resistance data on a computer. The smallest instantaneous radius of curvature of the film was estimated from photographs taken of the side view of the film in bending. Development of sheet resistance during tensile deformation was examined similarly. Testing was carried out by cyclically loading and unloading either only in the elastic region (from 0% to 0.5% tensile strain and back at a deformation rate of 20 µm s^{-1}) or also in the plastic region (deformation rate 8.35 µm s^{-1}) by increasing the maximum strain 1% unit per cycle.

Supporting Information

Supporting Information is available from the Wiley Online Library or from the author.

Acknowledgements

M.S.T., O.J.R. and O.I. acknowledge the Academy of Finland Centres of Excellence Programme (2014–2019) as this work was supported by the Academy of Finland project 264677. A.K. and E.I.K. acknowledge Aalto University (MOPPI project in AEF program), JST-EC DG RTD Coordinated Research Project "IRENA," TEKES funded project "CARLA," and Academy of Finland project "HISCON." This work made use of the Aalto University Nanomicroscopy Center (Aalto-NMC) premises. The authors acknowledge Michael Treacy of his help with the SWNT synthesis and sample preparation.

Received: June 23, 2015
Revised: August 26, 2015
Published online: September 28, 2015

[1] L. W. Hrubesh, J. F. Poco, *J. Non. Cryst. Solids* **1995**, *188*, 46.
[2] L. W. Hrubesh, *J. Non. Cryst. Solids* **1998**, *225*, 335.
[3] A. C. Pierre, G. M. Pajonk, *Chem. Rev.* **2002**, *102*, 4243.
[4] D. Zhang, L. Shi, J. Fang, K. Dai, X. Li, *Mater. Chem. Phys.* **2006**, *97*, 415.
[5] X. Gui, J. Wei, K. Wang, A. Cao, H. Zhu, Y. Jia, Q. Shu, D. Wu, *Adv. Mater.* **2010**, *22*, 617.
[6] S. B. Riffat, G. Qiu, *Int. J. Low Carbon Technol.* **2012**, *8*, 1.
[7] S. N. Schiffres, K. H. Kim, L. Hu, A. J. H. McGaughey, M. F. Islam, J. A. Malen, *Adv. Funct. Mater.* **2012**, *22*, 5251.
[8] Z. Sui, Q. Meng, X. Zhang, R. Ma, B. Cao, *J. Mater. Chem.* **2012**, *22*, 8767.
[9] Z. Xu, Y. Zhang, P. Li, C. Gao, *ACS Nano* **2012**, *6*, 7103.
[10] N. Gaponik, A.-K. Herrmann, A. Eychmüller, *J. Phys. Chem. Lett.* **2012**, *3*, 8.
[11] C. Tan, B. M. Fung, J. K. Newman, C. Vu, *Adv. Mater.* **2001**, *13*, 644.
[12] M. B. Bryning, D. E. Milkie, M. F. Islam, L. A. Hough, J. M. Kikkawa, A. G. Yodh, *Adv. Mater.* **2007**, *19*, 661.
[13] M. Pääkkö, J. Vapaavuori, R. Silvennoinen, H. Kosonen, M. Ankerfors, T. Lindström, L. A. Berglund, O. Ikkala, *Soft Matter* **2008**, *4*, 2492.
[14] R. T. Olsson, M. A. S. Azizi Samir, G. Salazar-Alvarez, L. Belova, V. Ström, L. A. Berglund, O. Ikkala, J. Nogués, U. W. Gedde, *Nat. Nanotechnol.* **2010**, *5*, 584.
[15] J. Zou, J. Liu, A. S. Karakoti, A. Kumar, D. Joung, Q. Li, S. I. Khondaker, S. Seal, L. Zhai, *ACS Nano* **2010**, *4*, 7293.
[16] J. T. Korhonen, P. Hiekkataipale, J. Malm, M. Karppinen, O. Ikkala, R. H. A. Ras, *ACS Nano* **2011**, *5*, 1967.
[17] H. Jin, M. Kettunen, A. Laiho, H. Pynnönen, J. Paltakari, A. Marmur, O. Ikkala, R. H. A. Ras, *Langmuir* **2011**, *27*, 1930.
[18] K. H. Kim, M. Vural, M. F. Islam, *Adv. Mater.* **2011**, *23*, 2865.
[19] Y. Fang, F. Jiang, H. Liu, X. Wu, Y. Lu, *RSC Adv.* **2012**, *2*, 6562.
[20] N. Hüsing, U. Schubert, *Angew. Chem. Int. Ed.* **1998**, *37*, 22.
[21] N. Leventis, C. Sotiriou-Leventis, G. Zhang, A.-M. M. Rawashdeh, *Nano Lett.* **2002**, *2*, 957.
[22] S. Mulik, C. Sotiriou-Leventis, G. Churu, H. Lu, N. Leventis, *Chem. Mater.* **2008**, *20*, 5035.
[23] D. J. Boday, P. Y. Keng, B. Muriithi, J. Pyun, D. A. Loy, *J. Mater. Chem.* **2010**, *20*, 6863.
[24] H. Maleki, L. Durães, A. Portugal, *Microporous Mesoporous Mater.* **2014**, *197*, 116.
[25] H. Sehaqui, Q. Zhou, L. A. Berglund, *Compos. Sci. Technol.* **2011**, *71*, 1593.
[26] H. Sehaqui, Q. Zhou, O. Ikkala, L. A. Berglund, *Biomacromolecules* **2011**, *12*, 3638.
[27] H. Sehaqui, S. Morimune, T. Nishino, L. A. Berglund, *Biomacromolecules* **2012**, *13*, 3661.
[28] Y. Kobayashi, T. Saito, A. Isogai, *Angew. Chem. Int. Ed.* **2014**, *53*, 10394.
[29] S. Bandi, M. Bell, D. A. Schiraldi, *Macromolecules* **2005**, *38*, 9216.
[30] E. M. Arndt, M. D. Gawryla, D. A. Schiraldi, *J. Mater. Chem.* **2007**, *17*, 3525.
[31] K. Finlay, M. D. Gawryla, D. A. Schiraldi, *Ind. Eng. Chem. Res.* **2008**, *47*, 615.
[32] M. D. Gawryla, O. van den Berg, C. Weder, D. A. Schiraldi, *J. Mater. Chem.* **2009**, *19*, 2118.
[33] M. A. Worsley, P. J. Pauzauskie, S. O. Kucheyev, J. M. Zaug, A. V. Hamza, J. H. Satcher, T. F. Baumann, *Acta Mater.* **2009**, *57*, 5131.
[34] X. Gui, A. Cao, J. Wei, H. Li, Y. Jia, Z. Li, L. Fan, K. Wang, H. Zhu, D. Wu, *ACS Nano* **2010**, *4*, 2320.
[35] K. H. Kim, Y. Oh, M. F. Islam, *Nat. Nanotechnol.* **2012**, *7*, 562.
[36] C. Zhu, T. Y.-J. Han, E. B. Duoss, A. M. Golobic, J. D. Kuntz, C. M. Spadaccini, M. A. Worsley, *Nat. Commun.* **2015**, *6*, 6962.
[37] S. S. Prakash, C. J. Brinker, A. J. Hurd, S. M. Rao, *Nature* **1995**, *374*, 439.
[38] J. Fricke, *Nature* **1995**, *374*, 409.
[39] P. R. Aravind, P. Shajesh, G. D. Soraru, K. G. K. Warrier, *J. Solgel Sci. Technol.* **2010**, *54*, 105.
[40] R. D. Perlack, L. L. Wright, A. F. Turhollow, R. L. Graham, B. J. Stokes, D. C. Erbach, *Biomass as Feedstock for A Bioenergy and Bioproducts Industry: The Technical Feasibility of a Billion-Ton Annual Supply*, Technical Report of the U.S. Department of Commerce, Springfield, MA, USA **2005**.
[41] R. J. Moon, A. Martini, J. Nairn, J. Simonsen, J. Youngblood, *Chem. Soc. Rev.* **2011**, *40*, 3941.
[42] S. Tanpichai, F. Quero, M. Nogi, H. Yano, R. J. Young, T. Lindström, W. W. Sampson, S. J. Eichhorn, *Biomacromolecules* **2012**, *13*, 1340.
[43] T. Saito, R. Kuramae, J. Wohlert, L. A. Berglund, A. Isogai, *Biomacromolecules* **2013**, *14*, 248.
[44] N. Lin, A. Dufresne, *Eur. Polym. J.* **2014**, *59*, 302.
[45] M. Henriksson, L. A. Berglund, P. Isaksson, T. Lindström, T. Nishino, *Biomacromolecules* **2008**, *9*, 1579.
[46] Z. Wu, Z. Chen, X. Du, J. M. Logan, J. Sippel, M. Nikolou, K. Kamaras, J. R. Reynolds, D. B. Tanner, A. F. Hebard, A. G. Rinzler, *Science* **2004**, *305*, 1273.
[47] M. Kaempgen, G. S. Duesberg, S. Roth, *Appl. Surf. Sci.* **2005**, *252*, 425.
[48] A. G. Nasibulin, D. P. Brown, P. Queipo, D. Gonzalez, H. Jiang, E. I. Kauppinen, *Chem. Phys. Lett.* **2006**, *417*, 179.
[49] Y. Zhou, L. Hu, G. Grüner, *Appl. Phys. Lett.* **2006**, *88*, 123109.
[50] A. Kaskela, A. G. Nasibulin, M. Y. Timmermans, B. Aitchison, A. Papadimitratos, Y. Tian, Z. Zhu, H. Jiang, D. P. Brown, A. Zakhidov, E. I. Kauppinen, *Nano Lett.* **2010**, *10*, 4349.
[51] D.-M. Sun, M. Y. Timmermans, A. Kaskela, A. G. Nasibulin, S. Kishimoto, T. Mizutani, E. I. Kauppinen, Y. Ohno, *Nat. Commun.* **2013**, *4*, 2302.
[52] J. T. Hong, D. J. Park, J. H. Yim, J. K. Park, J.-Y. Park, S. Lee, Y. H. Ahn, *J. Phys. Chem. Lett.* **2013**, *4*, 3950.
[53] N. Fukaya, D. Y. Kim, S. Kishimoto, S. Noda, Y. Ohno, *ACS Nano* **2014**, *8*, 3285.
[54] A. G. Nasibulin, A. Kaskela, K. Mustonen, A. S. Anisimov, V. Ruiz, S. Kivistö, S. Rackauskas, M. Y. Timmermans, M. Pudas, B. Aitchison, M. Kauppinen, D. P. Brown, O. G. Okhotnikov, E. I. Kauppinen, *ACS Nano* **2011**, *5*, 3214.
[55] M. Bhattacharya, M. M. Malinen, P. Lauren, Y.-R. Lou, S. W. Kuisma, L. Kanninen, M. Lille, A. Corlu, C. GuGuen-Guillouzo, O. Ikkala, A. Laukkanen, A. Urtti, M. Yliperttula, *J. Control. Release* **2012**, *164*, 291.
[56] L. Xu, S. R. Gutbrod, A. P. Bonifas, Y. Su, M. S. Sulkin, N. Lu, H.-J. Chung, K.-I. Jang, Z. Liu, M. Ying, C. Lu, R. C. Webb, J.-S. Kim, J. I. Laughner, H. Cheng, Y. Liu, A. Ameen, J.-W. Jeong, G.-T. Kim, Y. Huang, I. R. Efimov, J. A. Rogers, *Nat. Commun.* **2014**, *5*, 3329.
[57] Y.-R. Lou, L. Kanninen, T. Kuisma, J. Niklander, L. A. Noon, D. Burks, A. Urtti, M. Yliperttula, *Stem Cells Dev.* **2014**, *23*, 380.
[58] M. S. Toivonen, S. Kurki-Suonio, F. H. Schacher, S. Hietala, O. J. Rojas, O. Ikkala, *Biomacromolecules* **2015**, *16*, 1062.
[59] J. Prasek, J. Drbohlavova, J. Chomoucka, J. Hubalek, O. Jasek, V. Adam, R. Kizek, *J. Mater. Chem.* **2011**, *21*, 15872.
[60] H. Koga, M. Nogi, N. Komoda, T. T. Nge, T. Sugahara, K. Suganuma, *NPG Asia Mater.* **2014**, *6*, e93.
[61] L. Cai, J. Li, P. Luan, H. Dong, D. Zhao, Q. Zhang, X. Zhang, M. Tu, Q. Zeng, W. Zhou, S. Xie, *Adv. Funct. Mater.* **2012**, *22*, 5238.
[62] S. Brunauer, P. H. Emmett, E. Teller, *J. Am. Chem. Soc.* **1938**, *60*, 309.
[63] E. P. Barrett, L. G. Joyner, P. P. Halenda, *J. Am. Chem. Soc.* **1951**, *73*, 373.
[64] S. M. Kim, K. K. Kim, Y. W. Jo, M. H. Park, S. J. Chae, D. L. Duong, C. W. Yang, J. Kong, Y. H. Lee, *ACS Nano* **2011**, *5*, 1236.